

Thermal Properties, Microstructure and Microhardness of Cu–Al–Co Shape Memory Alloy System

Yıldırım Aydoğdu · Ferdi Kürüm · Mediha Kök ·
Zehra Deniz Yakinci · Ayşe Aydoğdu

Received: 14 August 2013 / Accepted: 20 December 2013 / Published online: 9 March 2014
© Indian Institute of Metals 2014

Abstract In this study, the effects of Co content on the crystal structure, transformation temperatures and microstructure of Cu–Al–Co shape memory alloy system were investigated. It was found that Cu–Al–Co alloy system has also 18R type martensitic structure, which is commonly observed in copper-based systems. The transformation temperatures were found to be higher than 250 °C and they do not show a linear increase or decrease with Co content. The microstructural examination revealed the presence of martensite phase and precipitates. It was realized that the size of precipitate increases with increasing Co content. It can be stated that the hardness increased with increasing Co content. All these results point out that increasing Co content increases the strength of Cu–Al–Co shape memory alloy system.

Keywords Shape memory alloys · Precipitate · Martensite · Vickers hardness

Y. Aydoğdu (✉) · A. Aydoğdu
Faculty of Science, Department of Physics, Superconductivity
and Thermal Analysis Laboratory, Gazi University, Ankara,
Turkey
e-mail: y.aydogdu@gazi.edu.tr

A. Aydoğdu
e-mail: a.aydogdu@gazi.edu.tr

F. Kürüm · M. Kök
Department of Physics, Sciences Faculty, Firat University,
Elazığ, Turkey
e-mail: ferdikurum@hotmail.com

M. Kök
e-mail: msoglu@firat.edu.tr

Z. D. Yakinci
Vocational School of Health Service, Inonu University, Malatya,
Turkey
e-mail: Deniz.yakinci@inonu.edu.tr

1 Introduction

Copper-based alloys are a group of alloys, which are preferred in technological applications due to their high thermal and electrical conductivities. Ni–Ti, Cu and Fe-based shape memory alloys are being used for many commercial applications due to their unique shape memory properties. Cu-based alloys are less expensive than Ni–Ti alloys and also demonstrate better shape memory effect and superelasticity than Fe-based alloys [1]. As a result of these superior properties, Cu-based alloys are frequently demanded to use in engineering applications. However, some Cu-based shape memory alloys, such as Cu–Al–Ni and Cu–Al–Zn, are extremely brittle [1]. Cu–Al alloys show superior strength and corrosion resistance while demonstrating limited shape memory effect [2]. The shape memory behavior of these alloys allows them to be used in a variety of applications, i.e., orthodontic devices, glass frames, antennae for mobile phones, catheters and stents [3], sensors and actuators [4].

Rapid cooling of the Cu–Al alloys with Al content between 9 and 14 at.% from high temperature yields martensitic phase transformation and aging of martensite results in formation of the eutectoid phase ($\alpha + \gamma_1$) in these alloys [3]. When the electron concentration of Cu–Al alloys is between 1.40 and 1.55 (including both values), disordered BCC phase becomes stable at high temperature [5]. Therefore, the Cu based alloys exhibit shape memory affect at this e/a ratio. There are two possible ordering mechanisms in an alloy with a Cu_3Al composition. The first one is the transformation from disordered BCC-type (A2) structure to the CsCl-type (B2) structure at 973 K (700 °C), and the second one is the ordering transformation from B2 structure to the DO_3 structure at 843 K [5].

In the literature, many studies can be found in which a third element is added to the Cu–Al-based alloys [5–7]. Ni, Mn and Be were frequently used for this purpose [8–13]. The main purpose of the addition of these elements is to decrease the transformation temperatures of Cu–Al alloys. However, limited number of studies have been carried out on the addition of Fe, Co, Ag. Silva et al. [3] examined the effects of Ag addition on the properties of a Cu–Al alloy. In one of these studies, it was found that the decomposition reaction of the (β_1) parent phase is decreased and the effect of martensite stabilization is influenced by the addition of Ag [3]. In another Silva et al. [14] study they have found that the addition of Ag does not affect the phase transformation properties [14]. Carvalho et al. [2] also studied the effect of Ag addition on the properties of Cu–Al alloy and found that Ag addition influences the regular β phase as well as martensite phase transformation. Ma and co-workers [17] examined the martensite transformation and thermal stability of Cu–Al–Co and Cu–Al–Zr alloys. They found that the transformation temperatures of these alloys were higher than 200 °C and that these alloys demonstrated better shape memory property. Thermal cycling was applied to these alloys by DSC, which demonstrated that the martensite transformation diminished after five cycles in Cu–Al–Co alloy and after two cycles in Cu–Al–Zr alloy [15].

In shape memory alloys, cobalt addition is applied to improve the thermal stability and reduce the inverse martensite transformation temperatures. Meanwhile, cobalt was frequently added into the Cu-based shape memory alloys to control the grain size, reduce the grain growth rate and increase the strength [16, 17]. However, there are limited numbers of studies on the cobalt addition to Cu-based alloys. In this study, four select alloys in Cu–Al–Co systems were investigated to examine the effects of cobalt addition on their shape memory properties.

2 Experimental

The alloy compositions given in Table 1 were prepared by using 99.9 % pure Cu, 99.9 % pure Al, 99.9 % pure Co powders. The powders were mixed and subsequently compacted by applying a pressure of 1 ton. These pelletized powder mixtures were melted in an arc furnace and ingots were obtained. Remelting was done for a few times so as to increase the homogeneity of the samples. The homogenization of Cu–Al–Co shape memory alloy samples was done at 850 °C for 72 h after which they were immediately quenched into a water–ice–salt mixture.

In order to determine the final composition of the samples, EDX (Energy Dispersive X-Ray Spectroscopy)

Table 1 The amount of elements, in wt%, for alloys with nominal compositions

| Alloy code | Cu (wt%) | Al (wt%) | Co (wt%) |
|------------|----------|----------|----------|
| F1 | 86.5 | 13 | 0.5 |
| F2 | 86 | 13 | 1 |
| F3 | 85.5 | 13 | 1.5 |
| F4 | 85 | 13 | 2 |

analyses were performed using a SEM equipped with the EDX analyzer. The results of EDX analyses are given in Table 2. Differential scanning calorimeter (DSC) is the commonly used equipment to determine the phase transformation temperatures of shape memory alloys. DSC measurement of Cu–Al–Co alloy samples was performed under a protective N₂ atmosphere by Perkin Elmer Sapphire DSC at a constant heating/cooling rate of 25 °C/min.

XRD analysis was performed by using a Bruker Discover D8 X-Ray diffractometer employing Cu-K α radiation ($\lambda = 1.54178 \text{ \AA}$) at a scanning rate of 2°/min in the 2 θ range of 20°–80°. Phase transformations in the samples were determined by XRD analysis. Cold-cast polyester resin was applied to the Cu–Al–Co samples so as to obtain their microstructure by optical microscopy. After polishing the cold-cast samples, they were chemically etched using etchant containing 20 ml of HCl, 5 g of FeCl₃–H₂O and 96 ml of methanol. The etched samples were examined by using a Nikon Eclipse MA200 optical microscope. Microhardness measurements of the alloy samples were performed by using a Emco Test DuraScan microhardness testing machine.

3 Results and Discussions

XRD diffraction patterns of the Cu–Al–Co alloy system, obtained at room temperature, are given in the Fig. 1. The peaks were indexed according to the parameters given in the literature [18–21]. All alloys were found to have a β_1^I (18R) martensitic structure. While the peaks of main phase are stronger in intensity for F1 and F4, they are weaker for F2 and F3 alloys. The reason for the weak base peak is that amorphous phase is dominant peak. Amorphous phase presents splayed peak and the base phase peak is not blurry [22–24]. The reason for this amorphous phase is considered that the diffraction pattern of the alloy system was obtained from bulk specimen instead of powder form and the X-ray came across to precipitates resulted from Cobalt. If XRD peaks in the alloys F1 and F4 are compared, peaks from (128),(208) and (1210),(2012) planes are not clearly distinguishable in F1, while in F4, these peaks are split and become distinguishable.

Table 2 Results of the EDX analyses for Cu–Al–Co shape memory alloy system

| Alloy code | Cu | | Al | | Co | | e/a |
|------------|-------|--------|-------|--------|-------|--------|------|
| | (wt%) | (at.%) | (wt%) | (at.%) | (wt%) | (at.%) | |
| F1 | 88.43 | 76.95 | 10.98 | 22.50 | 0.59 | 0.56 | 1.46 |
| F2 | 88.52 | 77.63 | 10.58 | 21.23 | 1.20 | 1.13 | 1.44 |
| F3 | 86.25 | 75.37 | 10.47 | 21.54 | 3.29 | 3.10 | 1.49 |
| F4 | 84.97 | 74.32 | 10.31 | 21.23 | 4.73 | 4.46 | 1.51 |

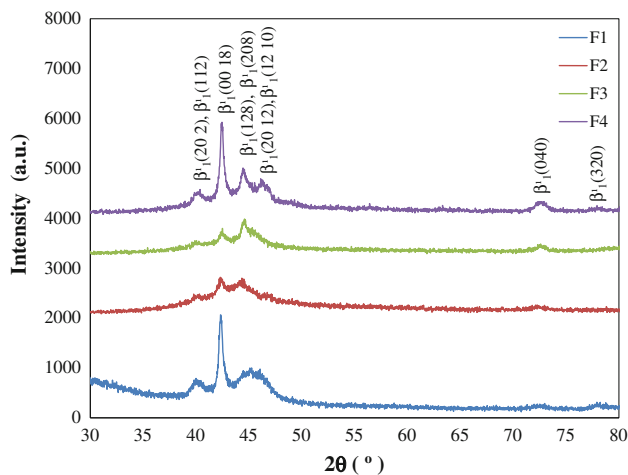


Fig. 1 XRD pattern of the Cu–Al–Co shape memory alloy system

Results of the DSC measurements of four select Cu–Al–Co alloys are given in Table 3. As an example, the DSC response of F2 is also demonstrated in Fig. 2. As for the Table, the austenitic transformation temperatures decrease with decreasing Co content. Meanwhile, there is a decreasing trend for the T_o . However, a stable increase or decrease in the transformation temperature with the variation of Co content is not observed. This is attributed to variation of Cu and Al contents while the Co content was changed. Thus, the variations in the transformation temperature could not simply be attributed to Co content.

The variation of austenite and martensite-transformation peak values with Co content is demonstrated graphically in Fig. 2. The peak value of the austenite temperature (A_p) decreases with Co content. However, the martensite peak

transformation (M_p) increases for F1 and F2, but decreases with Co content (Fig. 3).

From DSC measurements, the change in enthalpy and entropy during the phase transformations can be identified. The integral of the transformation peak in cooling and heating yields the change in enthalpy as a function of temperature. The average value of the enthalpy is found by the following equation;

$$\Delta H_{av} = (\Delta H_{heating} + \Delta H_{cooling})/2$$

The change in entropy, on the other hand, can be determined by dividing the average value of the enthalpy with equilibrium temperature, $T_o = 0.5(A_s + M_s)$.

For select cobalt concentrations, the change in enthalpy value for Cu–Al–Co alloys is given in Table 3. While the change in enthalpy and entropy values are almost the same for alloys F1, F2 and F3, they are lower for alloy F4. These results are coherent with the data given in the literature [15].

The microscopic examination of etched Cu–Al–Co alloy samples was performed by optical microscopy. Figure 4a–d shows the optical microscopic images of the Cu–Al–Co alloy samples at 1000× magnification. In Fig. 4a, there are different kinds of martensite plates between two grains. While parallel martensitic plates are observed in the grain with a light contrast, V-type and lath-type martensitic plates are present in the grain with a dark contrast [25]. Shear bands are between the parallel martensite plates present in the grain with a light contrast. These shear bands are apparent variations in the martensitic plates as a result of the sudden temperature change that occurs during rapid cooling of the alloys. Lath-like martensitic plates can be clearly seen in the dark regions. In Fig. 4, the main reason

Table 3 The variation of transformation temperatures with composition in Cu–Al–Co shape memory alloy system

| | A_s (°C) | A_p (°C) | A_f (°C) | M_s (°C) | M_p (°C) | M_f (°C) | T_o (°C) | ΔH_{av} (J/g) | ΔS (J/g °C) |
|----|------------|------------|------------|------------|------------|------------|------------|-----------------------|---------------------|
| F1 | 301.1 | 338.3 | 370.3 | 278.2 | 236.7 | 204.1 | 289.6 | 3.88 | 0.013 |
| F2 | 308.2 | 337.7 | 351.9 | 269.5 | 247.2 | 205.8 | 288.8 | 3.47 | 0.012 |
| F3 | 288.6 | 328.9 | 350.4 | 262.1 | 244.0 | 164.6 | 275.3 | 3.58 | 0.013 |
| F4 | 289.6 | 312.9 | 355.5 | 264.1 | 223.3 | 196.6 | 276.8 | 2.21 | 0.008 |

Fig. 2 DSC graph of the alloy F2 obtained in N₂ atmosphere. The heating and cooling rate was 25 °C/min for the measurements

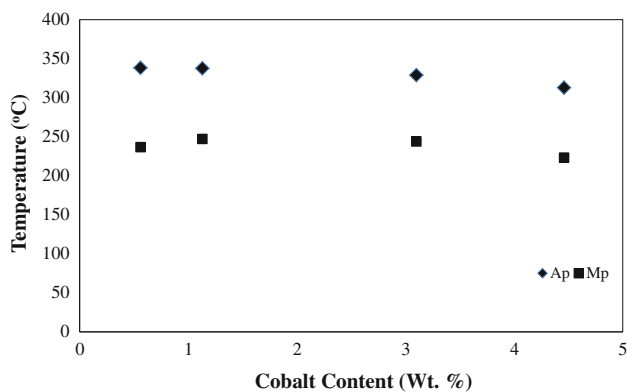
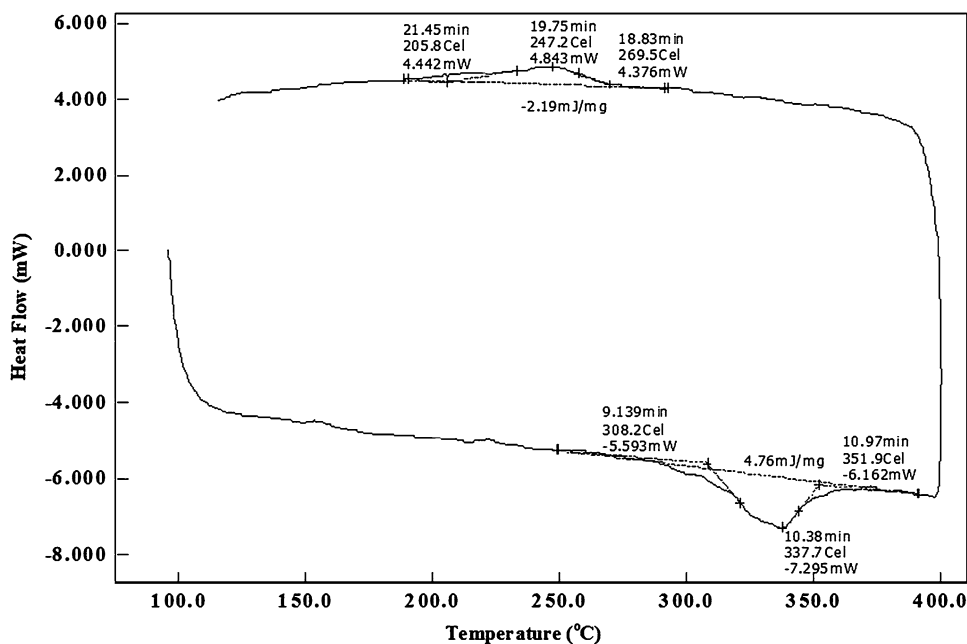


Fig. 3 The variation of peak temperature with the Co content in Cu–Al–Co shape memory alloys

for the formation of the light and dark regions, at left and right, respectively, is the different alignment of the martensitic plates. Precipitates were detected in all alloy systems examined, while they are not so clearly observable in F1 and F2. In F3 and F4, the size of the precipitate particles, which were shown arrow, increase with the increasing cobalt content. These precipitates mainly originate from Co.

Cu-based alloys showing thermoelastic martensite transformation are softer than Fe-based alloys. An important variation in the hardness of these alloys occurs with the formation of dislocations, textural distortion and addition of interstitial atoms. In this study, Vickers microhardness measurements were performed on the samples prepared for

optical microscopic examination. For each sample, three measurements were performed and the results are tabulated in Table 4.

From the values presented in the Table 4, it is clear that F1, the alloy with lowest Co content among all samples examined, possesses the lowest microhardness value. For this sample, images were taken from both light and dark grains. These measurements show that these two distinct grains have nearly equal microhardness values, indicating that both grains have the same phases (matrix phase), while the variation in color is mainly due to the alignment of the martensitic plates. In alloy F2 also, microhardness measurements were taken from different regions and it was found that the microhardness values were almost the same. Similar to alloy F1, small amount of precipitates were also detected in alloy F2, while it was not possible to measure their microhardness values due to their small size. The hardness value of the alloy F2 is higher than F1. In addition to these, microhardness values of the precipitates in alloys F3 and F4 were measured and it was found that the hardness values were higher. If the hardness values of precipitates are also considered in the calculation of average hardness values, it is found that the microhardness value of the alloy F4 is much higher than that of F1, F2 and F3. Thus, it can be concluded that the microhardness value increases with increasing cobalt addition. This result is coherent with the data given in the literature [17]. Cobalt is a 3d transition metal and is frequently added to Cu-based shape memory alloys to increase the strength [17].

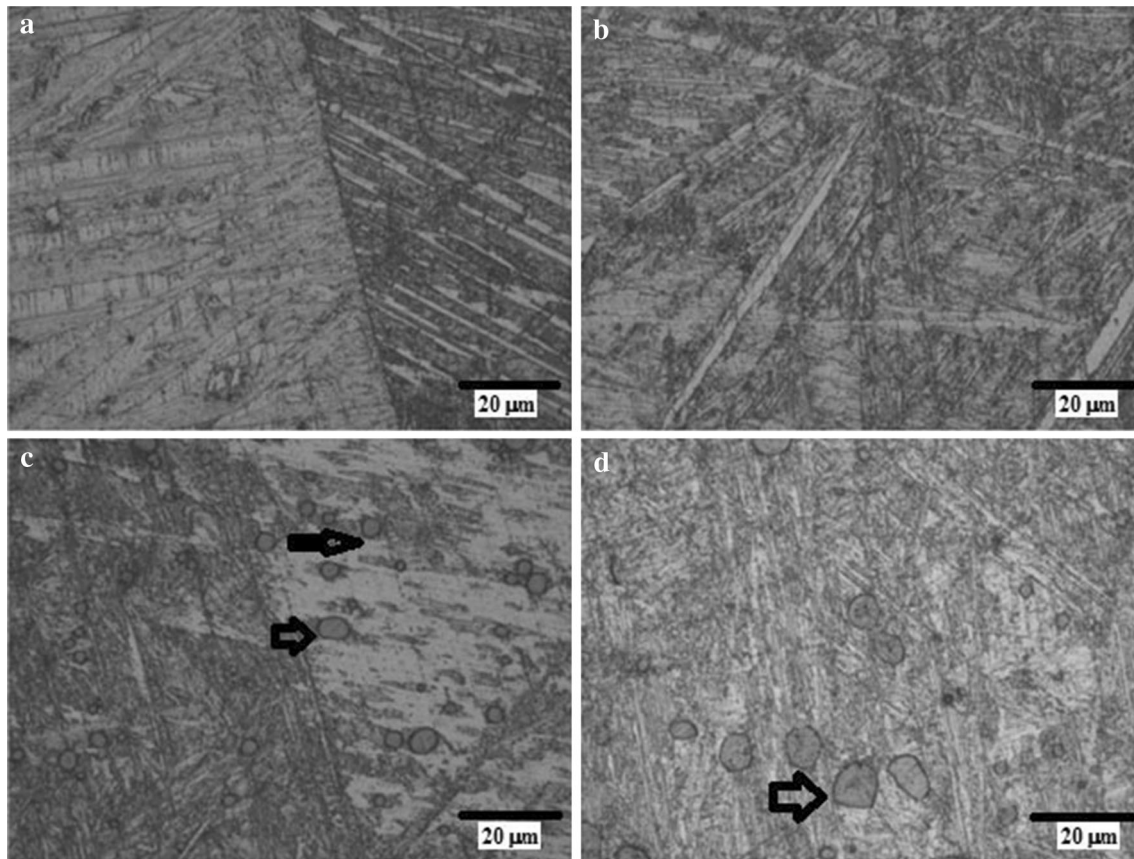


Fig. 4 Optical micrographs of alloys F1, F2, F3 and F4

Table 4 The variation of microhardness with composition in the Cu–Al–Co shape memory alloy system

| Alloy code | Hardness value of matrix (Hv) | Hardness value of precipitate (Hv) |
|------------|-------------------------------|------------------------------------|
| F1 | 219 | – |
| F2 | 306 | – |
| F3 | 282 | 485 |
| F4 | 295 | 734 |

4 Conclusions

The effects of Co addition on properties of Cu–Al–Co shape memory alloy system were investigated. The results can be outlined as follows:

- (a) The crystal structure examination of the Cu–Al–Co shape memory alloys with four different Co contents, reveals that all alloys yield characteristic peaks of 18R type martensite phase. The presence of an amorphous phase was also found by the XRD analysis

in all samples. This was attributed to precipitates originating from cobalt.

- (b) It was found that all alloys examined in the Cu–Al–Co shape memory system possess transformation temperatures higher than 250 °C. This points out that these alloys could be used as high temperature shape memory alloys. On the other hand, there is no definite correlations between cobalt content and transformation temperature. This can be attributed to variation of Cu and Al contents while the Co content is changed.
- (c) The microstructural analysis of the alloys examined within this study demonstrated the presences of martensitic phase (matrix phase) and precipitates. It was clearly observed that the size of precipitate particles increase with increasing Co content. Meanwhile, microhardness tests of four alloys demonstrate that the hardness values increase with increasing size of the precipitate particles.

Acknowledgments This work is supported by TUBITAK under project no: 106T583 and Firat University Research-Project unit under Project No: FF. 12.08.

References

1. Raju T M and Sampath V, *J Mater Eng Perform* **20** (2011) 767.
2. Carvalho T M, Silva R A G and Adorno A T, *J Therm Anal Calorim* **1** (2009) 53.
3. Silva R G A, Cuniberti A, Stipcich M and Adorno A T, *Mater Sci Eng A* **456** (2007) 5.
4. Lazzini F, Romero R and Castro M L, *Intermetallics* **16** (2008) 1090.
5. Vajpai S K, Dube R K and Sharma M, *J Mater Sci* **44** (2009) 4334.
6. Ochoa-Lara M T, Flores-Zuniga H and Rios-Jara D, *J Mater Sci* **41** (2009) 5455.
7. Gao Z Y, Wu Y, Tong Y X, Cai W, Zheng Y F and Zhao L C, *J Mater Sci* **41** (2006) 6165.
8. Vajpai S K, Dube R K and Sangal S, *Mater Sci Eng A* **570** (2013) 32.
9. Montecinos S and Simison S (2013) *Corros Sci* **74** (2013) 387.
10. Sutou Y, Omori T, Kainuma R and Ishida K, *Acta Mater* **61** (2013) 3842.
11. Lopez-Ferrenoa I, Breczewskib T, Ruiz-Larreab I, Lopez-Echarria A, Nób M L and San Juan J, *J Alloy Compd* (2012) doi: [10.1016/j.jallcom.2012.02.006](https://doi.org/10.1016/j.jallcom.2012.02.006).
12. Sade M, Yawnya A, Loveya F C and Torra V, *Mater Sci Eng A* **528** (2011) 7871.
13. Chang S H, *Mater Chem Phys* **125** (2011) 358.
14. Silva R A G, Paganotti A, Gama S, Adorno A T, Carvalho T M and Santos C M A, *Mater Charac* **75** (2013) 194.
15. Ma Y Q, Jiang C B and Xu H B, *Acta Metall Sin* **16–6** (2003) 445.
16. Funakoba H, *Shape Memory Alloys*, Kennedy J B, Gordon and Breach Science Publishers, London (1987).
17. Guilemany J M and Fernandez J, *J Mater Sci* **31** (1996) 4981.
18. Aydogdu A, Aydogdu Y and Adiguzel O, *J Mater Process Tech* **153–154** (2004) 164.
19. Zhang G F, Sauvage X, Wang J T and Langdon T G, *J Mater Sci* (2013) Doi:[10.1007/s10853-013-7153-8](https://doi.org/10.1007/s10853-013-7153-8).
20. Lojen G, Gojić M and Anžel I, *J Alloy Compd* (2013) doi: [10.1016/j.jallcom.2013.06.136](https://doi.org/10.1016/j.jallcom.2013.06.136).
21. Izadinia M and Dehghani K, *Trans. Nonferrous Met Soc China* **21** (2011) 2037.
22. Amini R, Mousavizad S M M, Abdollahpour H, Ghaffari M, Alizadeh M and Okyay A K, *Adv Powder Technol* (2013) [10.1016/j.appt.2013.03.005](https://doi.org/10.1016/j.appt.2013.03.005).
23. Amini R, Shamsipoor A, Ghaffari M, Alizadeh M and Okyay A K, *Mater Charac* **84** (2013) 169.
24. Kim M S, Jeon Y M, Im Y M, Lee Y H, and Nam T H, *Transition Electr Electron Mater*, **12–1** (2011) 20.
25. Ma Y, Jiang C, Deng L and Xu H, *J Mater Sci Technol* **19–5** (2003) 431.